Journal of Energy Storage 77 (2024) 109900

Contents lists available at ScienceDirect

Journal of Energy Storage

journal homepage: www.elsevier.com/locate/est

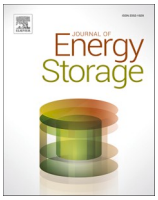

Research papers

NaOH protective layer for a stable sodium metal anode in liquid electrolytes

Alexander Thomas *, Björn Pohle, Johannes Schultz, Martin Hantusch, Daria Mikhailova *

Leibniz Institute for Solid State and Materials Research (IFW) Dresden e. V., Helmholtzstraße 20, 01069 Dresden, Germany

ARTICLE INFO

Keywords:
Sodium metal anode
Sodium dendrite
Sodium metal batteries
Sodium morphology

ABSTRACT

Sodium is known as a soft metal that can easily change its particle morphology. It can form outstretched and rolled fibers with plastic or brittle behavior, and cubes. In Na-batteries, metallic Na anodes demonstrate a high reactivity towards the majority of electrolyte solutions, volume change and a random deposition process from the electrolyte, accompanied by dendrite formation.

In order to smooth the electrochemical Na deposition, we propose NaOH as a simple artificial protective layer for sodium, formed by its exposure to ambient conditions for a certain period of time. The formed NaOH layer on top of the metallic sodium suppresses the volume change and dendrite growth on the sodium surface. Additionally, the protected sodium does not change its morphology after a prolonged contact with carbonate-based electrolytes. In symmetric Na-batteries, the NaOH layer increases the lifetime of the electrochemical cell by eight times in comparison to non-protected Na.

In the full-cell with a layered sodium oxide cathode, the NaOH-protected sodium anode also leads to a high cycling stability, providing 81 % of the initial cell capacity after 500 cycles with a 1C current rate. In contrast, batteries with a non-protected Na-anode reach only 20 % of their initial capacity under the same conditions. Therefore, the main benefits of the NaOH artificial layer are the chemical compatibility with the carbonate-based electrolytes, the protection of Na metal against reaction with the electrolyte solution, the rapid Na-ion diffusion through the layer and the formation of a mechanical barrier, mitigating Na-dendrite growth.

This work presents an easily scalable method to protect sodium without any additional chemicals or a special environment for this reaction.

1. Introduction

The development and establishment of sodium batteries in the market is a crucial step to achieve a constant energy supply in the future [1]. Especially in the case of intermittent renewable energy production, a storage system must be implemented to meet the requirements of industry and private households [2].

The initial step to attain the long-term objective is to implement sodium-ion-batteries (SIBs) with a hard carbon [3] anode, as a competitor to lithium-ion-batteries (LIBs) in the market [4]. However, hard carbons still have shortcomings, such as insufficient rate capability and low cycling stability [5].

Considering this aspect, more studies of anode materials for sodium batteries are necessary. Currently, investigations are focused on titanium-based oxides [6–13], metals like Sn, Sb, Ge, Pb, Zn or their sodium alloys [14,15], or two-dimensional (2D) transition metal dichalcogenides [16–19] as anode materials for long-time stable SIBs.

The anodes for a SIB need to fulfill special criteria like the ability to tolerate mechanical deformations [20], withstand a chemical reactive environment [21], a high ionic conductivity and low diffusion barrier [22]. However, all materials studied until now lack some of these properties. For example, titanium-based oxides have a low electronic conductivity and cycling stability, sodium-metal alloys feature huge volume changes upon (de)sodiation, while 2D transition metal dichalcogenides undergo phase transitions during cycling, resulting in the formation of new grain boundaries and impeded kinetics [23].

From an industrial point of view, the current knowledge of the majority of these materials does not allow their application as anodes in the near future. Moreover, several production steps are typically necessary to produce adequately protected and functional anodes as reported so far in the literature [23].

With the focus on the mentioned materials, metallic sodium is not

* Corresponding authors.
E-mail addresses: alexander.thomas@ifw-dresden.de (A. Thomas), d.mikhailova@ifw-dresden.de (D. Mikhailova).

https://doi.org/10.1016/j.est.2023.109900
Received 9 October 2023; Received in revised form 14 November 2023; Accepted 27 November 2023
Available online 2 December 2023

considered for usage in SIBs within the next years [24]. This is especially understandable with the electrochemical properties of sodium in mind. Sodium is a soft metal with a tendency to form dendrites and to exhibit large volume changes during cycling as anode in a battery with liquid organic electrolytes. Moreover, it generally has a high reactivity in contact with a lot of electrolytes, leading to irreversible electrolyte consumption and an instable solid-electrolyte interface (SEI) [25,26]. Therefore, none of the above-mentioned criteria for a robust and effective Na-battery anode are fulfilled.

However, studying metallic sodium anodes in batteries with liquid organic electrolytes is an important part for the future battery development, because only with this way the maximum possible energy density of sodium can be utilized in Na-cells [27].

Using metallic sodium as an anode represents an additional challenge. The non-uniform sodium deposition and the large volume change of metallic sodium shorten the cell life-time [28]. A possible way to overcome this issue is the application of an artificial SEI prior to the assembly of metallic sodium in the cell. The artificial SEI could be inorganic [29], organic [30] or hybrid [31] (inorganic and organic). To date, these artificial SEIs are always a compromise between mechanical stability and conductivity [32].

Another possible protection mechanism is the design of 3D structures to obtain a uniform and regulated plating of the sodium during cycling. Again, there is the possibility of using an inorganic 3D network, such as 3D porous Cu [33] or Ni [34], or a 3D structure designed from organic material, such as coconuts [35].

With this work, we want to introduce a viable strategy to construct a stable Na-metal anode in SIBs, implying the formation of NaOH as a protective layer on top of metallic sodium, when exposed to ambient conditions. With this layer metallic sodium can be operated much longer in sodium-metal batteries.

With a deeper look, choosing NaOH as protective layer is obvious, since it satisfies requirements for a stable SEI [36]. It is electronically insulating, builds a dense homogeneous film with a higher Young's modulus of ~31 GPa compared [37] to the Young's modulus of sodium with at least of 5 GPa [37] on the Na-surface [38] and is insoluble in commonly used organic electrolytes. Unfortunately, no sodium ionic conductivity data are available for solid NaOH in the literature. However, similarities in the NaOH and NaCl structure [39] (see Fig. 1a,b), where a significant sodium ionic conductivity is proven [40], allow a suggestion about sufficient Na-diffusivity in NaOH as well.

The formation of NaOH on the surface of metallic sodium was previously studied in 1934[41] with a lot of detailed work done by *S. Yamaguchi* in the 1940s [42–45]. It was found that multiple reactions take place, when sodium is exposed to air. Prior to NaOH formation, most likely Na_2O forms first. Formation of Na_2O_2 cannot be ruled out in presence of excess of oxygen. NaO_2 probably does not form, since higher temperatures are needed for the synthesis of this compound [46]. Next, NaOH is formed through the reaction of the oxide/peroxide with air humidity, followed by a subsequent reaction with carbon dioxide, eventually leading to the formation of $NaHCO_3$ after several minutes. Interestingly, the reaction of Na with oxygen and NaOH formation are catalyzed by impurities and nitrogen molecules, which usually do not react with sodium [47–49].

Thus, the following reaction mechanism during Na exposure to air can be proposed:

$$4Na + O_2 \rightarrow 2Na_2O \quad (1)$$

$$2Na_2O + O_2 \rightarrow 2Na_2O_2 \quad (2)$$

$$Na_2O + H_2O \rightarrow 2NaOH \quad (3)$$

$$Na_2O_2 + H_2O \rightarrow 2NaOH + ½\ O_2 \quad (4)$$

$$NaOH + CO_2 \rightarrow NaHCO_3 \quad (5)$$

Processes (1) and (2) as well as (3) and (4) are concurrent, and most likely all four reactions take place simultaneously on the surface of metallic sodium.

A direct reaction of sodium with water leads to the formation of NaOH as well, but with H_2 evolving.

$$2Na + 2H_2O \rightarrow 2NaOH + H_2 \quad (6)$$

This reaction occurred, when NaOH was used for the first time as part of a passivation layer, in 2020. *V. Kumar* et al. [29] reported the formation of NaOH within a protective bilayer containing $NaNH_2$, for metallic Na anode, with a good cycling stability in a Na—S battery. This bilayer was created during reaction between Na and ammonia water vapor in a confined cavity. A Na-anode with only a NaOH monolayer, formed similarly with water vapor, showed lower cycling stability in comparison to the bilayer. This NaOH monolayer is dense, with a thickness of about 5 μm.

In our work, we discuss grave morphology changes in the Na subsurface region after its exposure to air for a short time, which lead to a significant enhancement of the electrochemical performance in Na-batteries. Different ways of the NaOH formation on the Na-surface unambiguously influence the morphology of the surface layer including hierarchical pore structure and pore size. Therefore, crucial parameters for Na-protection and its application as anode could be recognized. Furthermore, we demonstrate for the first time in situ structural studies of Na-deposition and stripping using XRD methods, and a big difference in behavior of protected and non-protected Na. This protective strategy can be tested in every laboratory and is easily applicable for the industrial production of protected sodium anodes. We show a noticeable improvement in capacity retention in full-cells with a sodium oxide cathode and NaOH-protected metallic Na-anode.

2. Methods and materials

2.1. Preparation of sodium

Sodium was cut from a sodium block (Alfa Aesar, 99.95 %) stored in

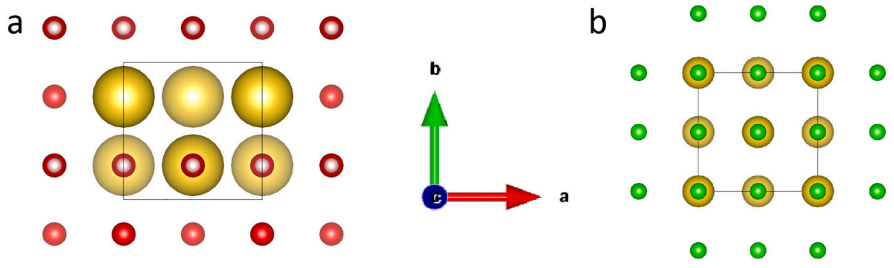

Fig. 1. View of the NaOH (a) and NaCl (b) structure in the ab-plane. Sodium (yellow) is in one plane with the anions (oxygen – red; chlorine – green) above and underneath (not visible). Light rosy spheres are H atoms in the NaOH structure. (For interpretation of the references to color in this figure legend, the reader is referred to the web version of this article.)

oil in an Ar-filled glove box ($O_2 < 0.1$ ppm, $H_2O < 0.1$ ppm). Prior to use, the sodium piece was washed with heptane, dried and cleaned by removing the light grey surface until metallic shine appears. For investigations, a small piece of sodium was rolled on a plate or directly onto a nickel current collector.

2.2. Preparation of NaOH passivation layer

The rolled sodium was exposed to ambient conditions for 5 s, until some small black dots are forming, and then transferred into the glove box. Exposure time was set as the time between opening and closing the transfer chamber of the glove box. On top, it contains a pure white layer. Transfer to FIB-SEM measurements, done with a Helios 5 CX instrument, exposes the formed layer to air for other 2–3 s.

2.3. Storage of passivated sodium in the electrolyte

A sodium chip with the NaOH layer was stored in 1 M $NaClO_4$ in EC/PC (1:1) for one week for XRD measurements.

2.4. Structural characterizations

Structural characterization was done at a STOE STADI/P powder diffractometer, using monochromatic Cu-Kα_1 or Mo-Kα_1 radiation. Samples were measured in the 2Θ scan mode between 10° and 80° (Cu) or between 2° and 50° (Mo). A continuous sample rotation was applied to minimize the texture effect.

For ex situ measurements, all samples with sodium were sealed within a Kapton foil, which ensures a measure time of nearly 3 h, before the characteristic NaOH peak at 38.2° 2Θ appears (in case of pure sodium) or grows (for passivated sodium). The change in the phase composition is a clear signal of a partial contact to the ambient atmosphere.

Scanning electron microscopy measurements were performed at a FEG-SEM, Zeiss Gemini 1530. For X-ray photoelectron spectroscopy (XPS), a PHI 5600 CI (Physical Electronics) instrument was used. As radiation source, Al-Kα (monochromatized) or Mg-Kα (satellite corrected) was used. All spectra were corrected to the binding energy of C1s at 284.8 eV. Due to the overlap of the Na AES (KLL) signal with O 1s using Al-Kα radiation, and overlap of the Na AES (KLL) signal with C 1s using Mg-Kα radiation, the O 1s peak was measured with Mg- and the C 1s peak with Al-radiation. Sample transport to the XPS device was done with an argon-filled transfer chamber (PHI model 04-110). SEM of bare sodium was performed at a JEOL JAMP 9500 instrument. The sample was transported to the SEM device inside an argon-filled transfer chamber (JEOL AP-Z08009TTRV). FIB-cut and FIB-SEM measurements were done with a Thermo Fisher Scientific Helios 5 CX.

For TEM measurements, an image corrected FEI Titan [3] at 300 kV acceleration voltage was used.

2.5. Electrochemical investigations

Electrochemical investigations were performed in coin cells of a 2032-type, and in Swagelok-type cells. As a separator, one layer of Whatman glass fiber was used for the coin cells and two layers for the Swagelok cells. Electrolyte in use was 1 M $NaClO_4$ in EC/PC (1:1).

As a cathode material, $Na_xCo_{0.8}Ti_{0.2}O_2$ (x = 0.7–0.8) [50] was chosen, mixed with 10 % PVDF binder (polyvinylidene difluoride, Solef 21216) and 10 % carbon (Super C65, TIMCAL) and coated on an aluminum foil; the loading of the active material was 1.6–1.7 mg/cm^2.

The battery cycling was performed galvanostatically with a constant current rate at a VMP3 Potentiostat (Bio-Logic SAS, Claix, France).

For the operando XRD analysis, a half-cell setup Na ‖ Na (passivated) with one passivated sodium electrode was cycled with a current density of ±2 mA/cm^2 flowing for 1 h. The cells with the Na-oxide cathode were galvanostatically cycled at a constant current density of 1C (256 mA/g), where 1C means the current for removal/insertion of 1 Na from/into $Na_xCo_{0.8}Ti_{0.2}O_2$ during 1 h.

3. Results

3.1. Sodium in the pristine state

The XRD results of sodium metal after rolling confirm a high crystallinity of the metal, showing, however, different reflection intensities in comparison to the literature data (Fig. 2a) [51]. Sodium crystallizes in a body-centered cubic unit cell (*bcc*), space group *Im*-3*m*, with the lattice parameter $a = 4.294$ Å. The intensity of the (110) peak is much higher than that of the (211) peak, giving the ratio of 10:1, in contrast to the literature data with a 5:1 to 3:1 ratio. Therefore, this might be a sign of the preferred orientation of Na particles in the (110) direction (Fig. 2b, Na after rolling). For clarity, Figs. 2c-f depicts a cubic structure of Na with marked lattice planes (110), (200) and (211).

In the phenomenological model of anisotropic peak broadening in powder diffraction [52], structural strains in a cubic crystal system can result in broadening of two groups of Bragg reflections. The first group includes reflections with (h00), (0h0) and (00h) Bragg indices, while the second group contains (hh0), (h0h) and (0hh) reflections. This approach is also applicable for materials with a certain particle morphology, since a pronounced intrinsic strain/stress will result in morphology changes of soft matter like Na. For example, prevalence of fibers in the material with a cubic lattice will lead to much higher intensities of (h00), (0 h0) and (00 h) reflections, whereas dominance of (hh0), (h0h) and (0hh) reflections points to plates or a bunch of highly oriented fibers. Therefore, increasing the (110) peak of Na under rolling corresponds to transformation of particles with a cubic shape to fibers/platelets aligned in one direction.

SEM photographs of partially pressed and rolled sodium reveal a rough surface area with cubic particles on it. Some fibers or wires incorporated into the surface structure become visible (Fig. 2a-b).

3.2. NaOH layer on the top of sodium

In agreement with the mechanism proposed in the introduction part, a NaOH layer forms on top of the rolled metallic sodium after 5 s exposure to air. This is visible by eye as a white surface and is confirmed by XRD analysis (Fig. 3a-b). Further investigations with SEM and FIB-SEM revealed a rough surface with a lot of pits and pores (Fig. 3c).

FIB-measurements show formation of two layers on the Na-surface as a result of air-exposure of Na. The first layer directly on the Na-surface consists of fine tubes of metallic Na with ca. 100 nm diameter. These tubes are interconnected by small, honeycomb-like fibers, forming some bigger caves, especially at the contact area to the metallic Na surface. The Na-fibers become denser and caves vanish with increasing distance to the metallic sodium surface and exposure time. A second surface layer of nearly 800 nm thickness appears at ca. 10 µm distance from the bulk Na surface, which is associated with the formation of NaOH (Fig. 3d-f).

The layer of nanosized sodium becomes denser with increasing distance to the metallic sodium surface and contact time to air. Therefore, the amount of nanocrystalline sodium is reversely proportional to the exposure time. The longer the surface is exposed to ambient conditions, the more nanocrystalline sodium transfers to macro-sized sodium. After a longer exposure time of 30 s, the layer on top of the metallic sodium is non-porous, containing a macro-sized structure, which is probably less accessible for sodium ions.

For the optimal time of Na exposure to air of 5 s, its volume expansion due to the formation of nanocrystalline Na in subsurface region and NaOH layer (800 nm) on top of it could be estimated as not higher than 3.5 % for the metallic chip with the initial thickness of 300 µm.

Different exposure times to air result in a change of Bragg reflection intensities of metallic Na, see for example the decrease of the Na (211) and increase of the (200) peak for exposure of 5 s and 30 s in Fig. 3b

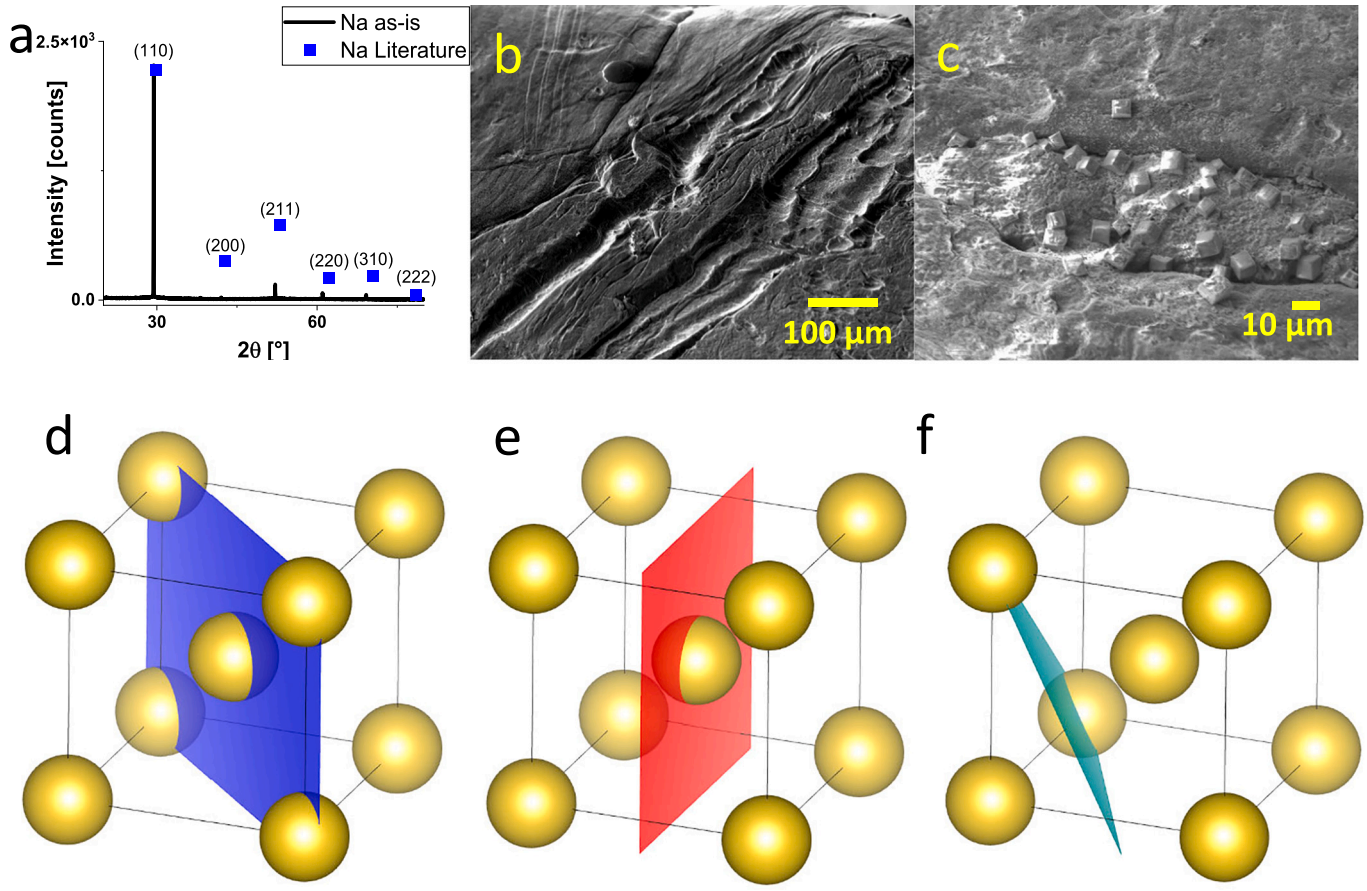

Fig. 2. (a-b) SEM of pristine sodium with (a) cubes and (b) fibers. c) XRD data of pristine sodium (Cu-Kα_1 radiation) together with the literature data (blue rectangles). At bottom there are the lattice planes (d) 110 (blue), (e) 200 (red, as a second order peak of 100) and (f) 211 (green) of sodium.

(more information in Section 5 of the supplement). Therefore, a transformation of particles with a cubic shape to fibers growing in one direction may occur. Increasing or decreasing in the intensity of the (110) peak is then an indicator for changes in agglomeration of highly oriented fibers, in accordance with the literature [53].

We would like to give a note of caution here. In principle, we have to be careful in drawing conclusions about the particle morphology based on the Bragg reflection intensities in the diffraction pattern of the soft Na metal being treated in a mechanical or chemical way. Very fast crystal growth of Na particles on the metal surface and a strong contribution from single-crystalline particles may result in adulteration of the diffractogram due to random error in the observed diffraction peak intensities. Ideally, an areal 2D detector would allow to distinguish between incomplete (spotty) Debye diffraction rings and texture (i.e. preferred crystallographic orientation).

TEM reveals polycrystallinity with grain sizes in the nanometer range at the surface of a sodium particle exposed to ambient conditions (Fig. 3g-h). The mean lattice plane distance was calculated to 0.35 nm +/− 0.05 nm out of a plot profile with 3.9 nm length covering 11 lattice planes (Fig. 3i). The relatively large uncertainty is caused by limited magnification of the lattice planes due to structural changes of the sodium particles induced by high electron dose at higher magnification. The determined lattice plane distance fits roughly with the *d*-spacing of 0.305 nm for the (110) direction of metallic sodium. [54,55]

As comparison the three *d*-spacings with highest intensity for NaOH (space group *Bmmb*) are 0.235 nm (111), 0.284 nm (004) and 0.568 nm (002) and deviate significantly from the measured value of 0.35 nm [39]. One can conclude that the investigated area contains only sodium, without any NaOH formed at this spot.

3.3. XPS measurements of bare and passivated sodium

Changes in the composition and binding energies of elements on the Na surface were evaluated with XPS measurements (Fig. 4a-c). All spectra were normalized for better comparison in intensity and corrected in binding energy by using the photoemission line of carbon (C1s) at 284.8 eV. The surface of the pristine Na chip mostly consists of sodium, oxygen and carbon. Besides the signal at 284.8 eV corresponding to -C-C- species, the C1s spectrum implies a second peak at 289.0 eV, which can be ascribed to a C═O bond. Together with the shoulder at a higher binding energy of 533.5 eV for the O1s peak, this species could represent some residuals on the sodium surface from cleaning or washing. During exposure to ambient conditions, the Na1s peak and the O1s peak shift both with about 0.7 eV to a higher energy (the shift is shown by blue and green lines). The peak shift of 0.7 eV for Na 1s between pristine state and 5 s contact to air agrees with a Na—O bond (in NaO_y or NaOH) formation, as reported in literature. [56,57] The slight shifts of the O1s and Na1s spectra, for the samples after 10 s contact to air, are due to the $NaHCO_3$ formation. XPS, like XRD data, confirms that the surface formation process of NaOH on top of metallic sodium is finished after nearly 5 s in air.

In the C 1s spectrum, the peak at 289.0 eV shifts to a higher binding energy of 289.6 eV after 5 s contact to air, although still representing the minor part of the surface carbon. The shift points to a subsequent carbon oxidation from C═O to O═C-OH species, standing for the formation of $NaHCO_3$ (more information in Section 3 and 4 of the supplement). This phase accumulates with time, since the peak becomes stronger in intensity after 10 s. An additional peak arises at 291.5 eV, in the C 1s spectra after keeping the Na chip for 1 s at ambient conditions, which is ascribed to a K2p signal (see Section 2 in the supplement for more

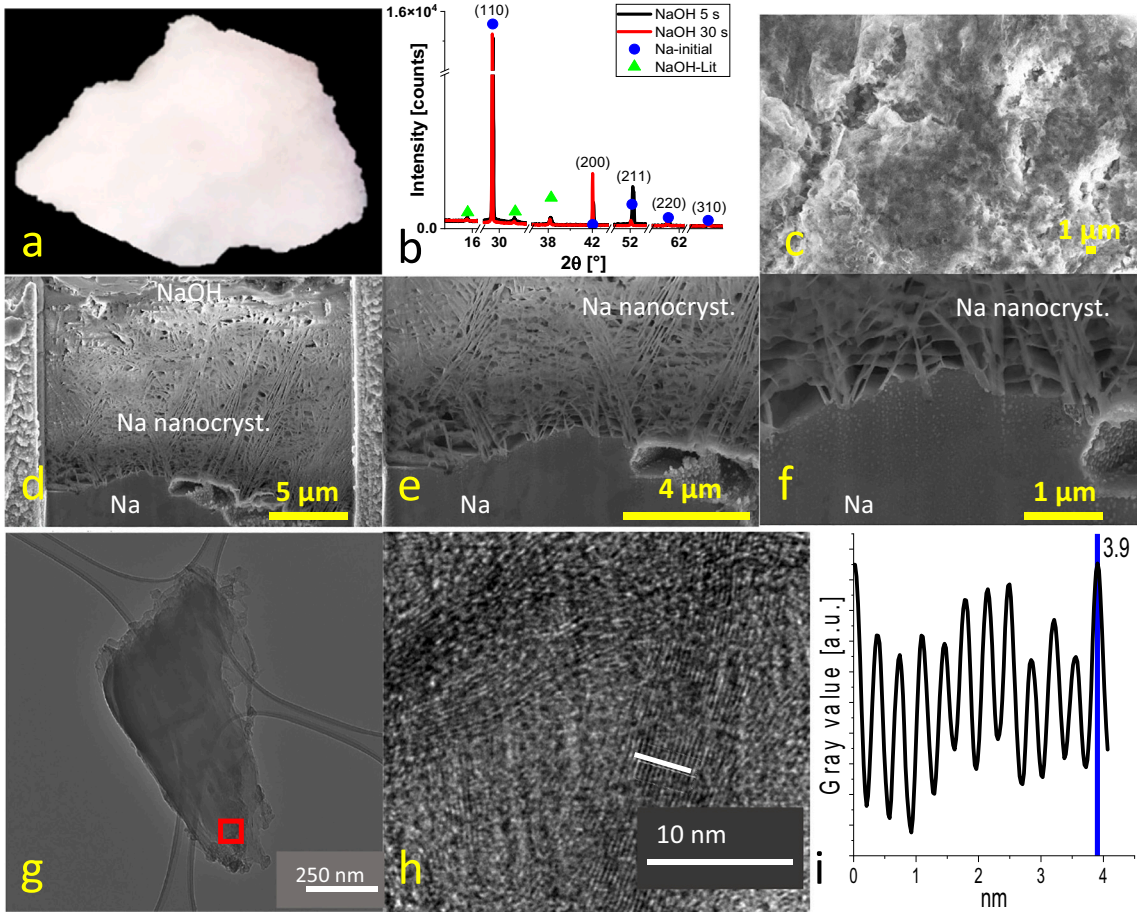

Fig. 3. (a) White film on sodium formed after exposure to air. (b) XRD patterns of a Na chip after different exposure time to air, together with Na and NaOH as references, recorded with Cu-Kα_1 radiation. (c) SEM of the NaOH layer. (d-f) FIB-SEM of the NaOH layer on top of metallic sodium after 5 s contact to air. Fibers in the surface region are clearly seen. These fibers are also visible in the HR-TEM pictures (g-h). (i) a plot profile over a length of 4 nm was measured along one of these fibers.

information).

XPS measurements prove the assumption that the exposure time of 5 s to ambient conditions is optimal. The formed film covers the whole surface and nearly no $NaHCO_3$ forms during this time.

3.4. Changes in Na metal morphology after electrolyte contact

Changes in the Na structure and morphology after contact to the electrolyte solution were evaluated for bare and NaOH-passivated sodium after storage in a 1 M $NaClO_4$ in EC/PC (1:1) electrolyte for one week (Fig. 5a,b).

The non-protected, bare sodium shows significant changes in color and morphology after one-week storage in the electrolyte (Fig. 5d,e). At the surface, brownish spots and black dots are visible. The XRD measurement reveals a significant intensity increase of the (200) and (211) reflections in comparison to a freshly prepared Na chip. Therefore, recrystallization of Na (repeated dissolution and deposition) at least in the sub-surface region occurred. The high (200) and (211) intensities with simultaneous decrease of the (110) peak may be an indicator for transformation of agglomerated fibers, highly orientated towards (hh0) direction (visible on the SEM photographs in Fig. 3c-h), to randomly distributed separated fibers, their breaking and finally to three-dimensional structures like cubes (211) in unprotected sodium in contact with the electrolyte.

In contrast, the NaOH-protected sodium remains white. Only small black dots appeared at the surface in some samples (Fig. 5f compared to Fig. 3a). SEM (Fig. 5g) shows nearly the same surface, like the original NaOH layer (Fig. 3c). The XRD data shows only a small change in the intensity of the (200) peak (red dot Fig. 5a), in comparison to the freshly protected sodium (black dot Fig. 5a). Therefore, NaOH cannot only withstand reactions with the electrolyte, but is also stable in contact to the sodium metal.

3.5. Electrochemical characterization

3.5.1. Half-cells Na ‖ Na (protected)

Electrochemical tests in a half-cell setup Na ‖ Na (NaOH-protected) were carried out in Swagelok cells using a galvanostatic mode with a current density of 1 mA/cm^2, 5 mA/cm^2 and 10 mA/cm^2 for a capacity of 1 mAh/cm^2. The experiment was stopped when the cell voltage reached 2 V (Fig. 6).

Common for the cells with the NaOH-protected Na (half-cells) is a noticeably longer lifetime of the half-cell setup in comparison to symmetric Na-cells with a non-protected Na. For a low current density of 1 mA/cm^2, the cell voltage in the symmetric Na-cell grew rapidly and reached 2 V after 23 cycles, pointing to a rapid increasing of the inner resistance in the cell, probably due to accumulated “dead” Na with a poor electrical contact to the current collector. The half-cell with the NaOH-protected Na is stable at this current density for at least 155 cycles. Afterwards, a very low cell voltage indicates a short circuit of the cell, probably due to a direct electrical contact between the electrodes. A higher current density generally leads to a shorter lifetime for symmetric and half-cell setups, but half-cells with the NaOH-protected Na still significantly overperform symmetric Na-cells with a non-protected Na.

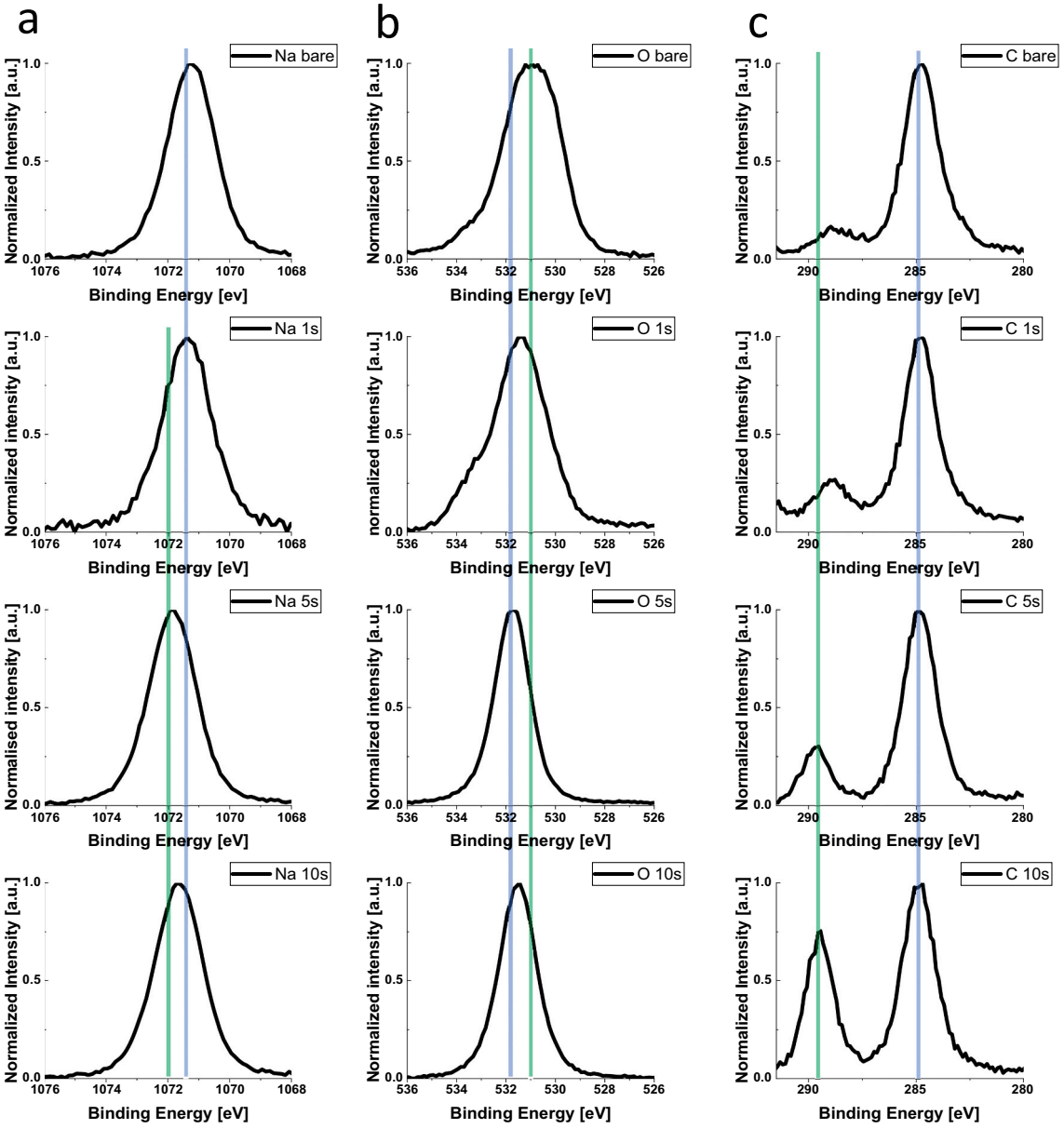

Fig. 4. XPS results (Mg-Kα radiation) of (a) Na1s, (b) O1s and (c) C1s for bare sodium (1st row) and sodium under ambient conditions for 1 s (2nd row), 5 s (3rd row), 10 s (last row). The Na1s, O1s and C1s signals shift to higher energies with increasing time. All spectra are C1s-corrected at 284.8 eV.

Thus, we observed an increase in cell operation from 10 cycles to 115 cycles at 5 mA/cm^2, and from 20 cycles to nearly 160 cycles at 10 mA/cm^2. The lifetime for three half-cells with the NaOH-protected Na-electrode is nearly 8-times higher than for a symmetric sodium cell.

Operando XRD analysis of repeated Na-deposition and -stripping in a symmetric Na and in a half Na ‖ Na (NaOH-protected) cell gives a deeper insight into the changes in morphology of sodium during cycling, and helps in answering the question, why a cell with NaOH-passivated sodium overperforms a symmetric sodium cell (Fig. 7).

With only small differences in the galvanostatic cycling (the *operando* cell with the passivated sodium has a slightly higher polarization of 0.4 V vs. 0.35 V at the beginning), the main changes are visible in the XRD data. Both cells show significant variations in the (110) peak intensity of Na. The cell with protected Na performs relatively constant in the first four Na deposition/stripping cycles, with a random intensity increase of the (110) peak in the fifth cycle. In contrast, the intensity of (110) peak of Na in the symmetric cell strongly varies with the cycling. Moreover, some peak broadening systematically appears, which arises from a random growth of Na-particles on top of Na and eventually from a more voluminous structure. Additionally, some non-systematic increasing intensity in the (211) direction is also observed for the non-protective Na.

Therefore, structural evolution of non-protected Na is probably associated with a random deposition of fibers and/or three-dimensional cube-like structures, what is usual in case of *bcc* metals [58,59]. A higher volume of deposited Na fibers can finally lead to a breaking of these fibers [60]. In contrast, one can conclude that NaOH-protection supports a regular Na-deposition and stripping without significant changes in the Na morphology.

3.5.2. *Protected sodium as electric conductor*

A facilitated charge transfer in case of NaOH-passivated Na against bare Na is also visible, when both Na-samples were investigated as electric conductors. The potential of the passivated sodium reached only 1/5 of the potential of bare sodium after applying the same current over the whole measurement time (Fig. 8).

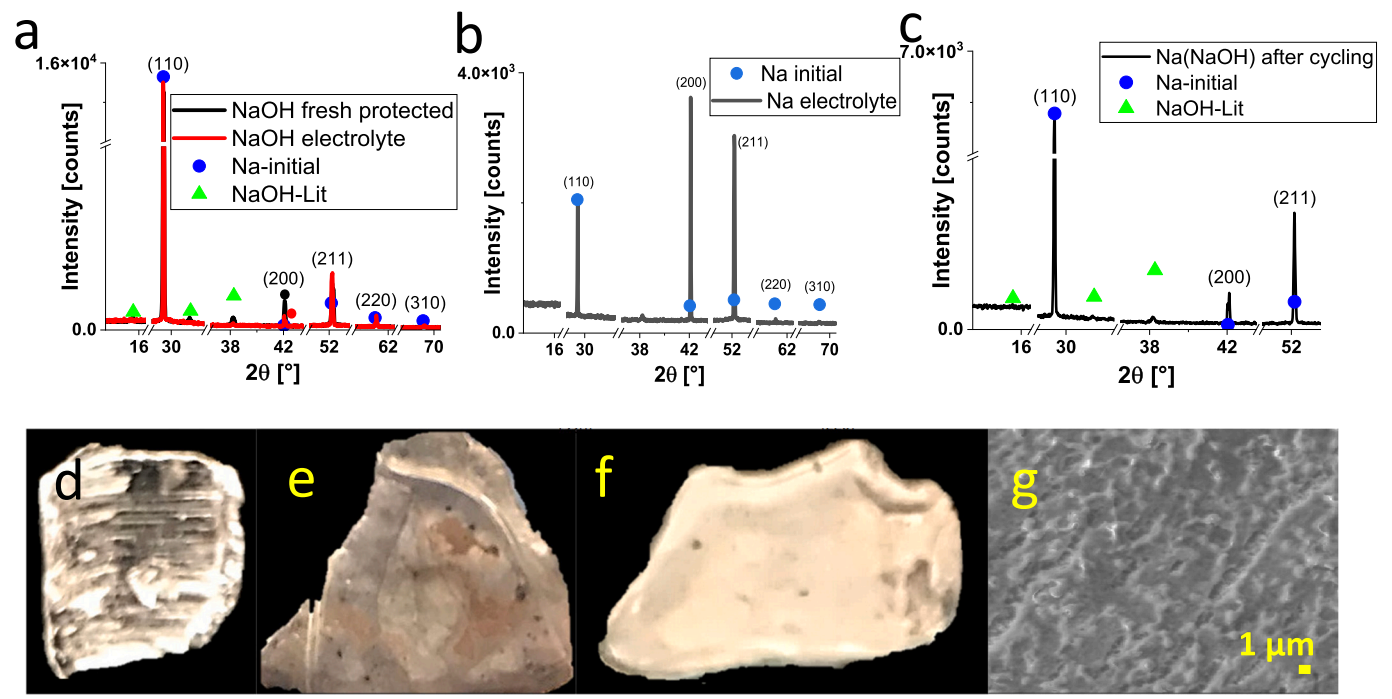

Fig. 5. X-ray diffraction patterns of Na after various treatments, measured with Cu-Kα1 radiation. (a) NaOH-protected sodium, (b) bare sodium, both stored in 1 M $NaClO_4$ in EC/PC electrolyte, and (c) protected sodium after 450 cycles in a half Na ‖ NaOH-Na cell. Surface of freshly cut metallic sodium (d) in comparison to unprotected sodium (e) and protected sodium (f) stored in electrolyte for one week. SEM of passivated sodium stored in electrolyte (g) shows a smooth surface, comparable with the original NaOH layer (Fig. 3c).

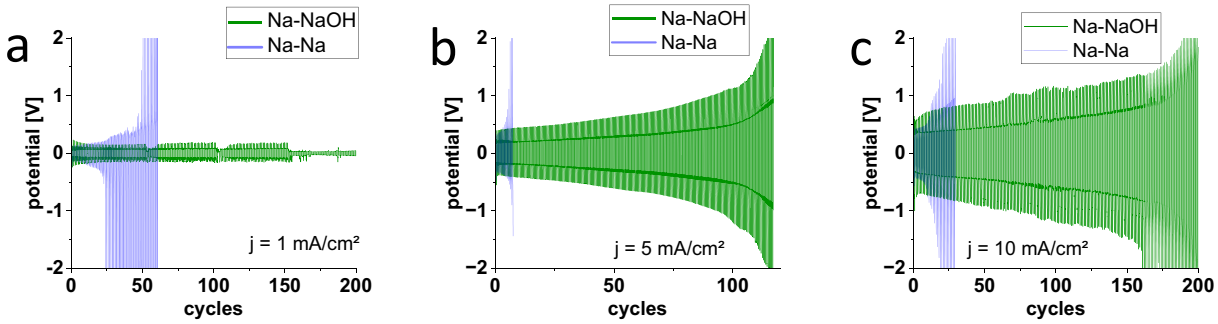

Fig. 6. GCPL of half-cells Na ‖ Na (NaOH-protected) with a current density of (a) 1 mA/cm^2, (b) 5 mA/cm^2 and (c) 10 mA/cm^2, for a total capacity of 1 mAh/cm^2.

This reflects a lower charge transfer resistance during cycling using NaOH-passivated sodium. The XRD patterns of NaOH-Na show only the very pronounced (110) reflection without any changes in intensity during the cycling time, confirming a stable Na morphology. The XRD patterns of bare Na demonstrates two very intense (110) and (200) reflections, with intensity variation of the (110) during the measurements. Therefore, some changes in the morphology of bare Na cannot be ruled out, probably due to a higher inner resistance and, therefore, a higher heating effect produced by the electric current (Joule's equation).

3.5.3. *Full-cell Na (NaOH-protected) ‖ $Na_xCo_{0.8}Ti_{0.2}O_2$ (x = 0.7 - 0.8)*

Both bare Na and NaOH-protected Na were tested as anode materials in full-cells with a $Na_{0.7}Co_{0.8}Ti_{0.2}O_2$ cathode [50] and a 1 M $NaClO_4$ in EC/PC electrolyte solution. A high chemical and mechanical stability of the NaOH-passivated Na-anode facilitates a stable electrochemical process in the full-cell arrangement, leading to a capacity retention of 81 % after 500 cycles at a 1C current density (cell charge and discharge in 1 h) upon room-temperature operation (Fig. 9 left).

In contrast, cells with a bare Na-anode demonstrate much faster capacity loss with the cycling, reaching 20 %–22 % of the initial capacity after 500 cycles at the same 1C current density.

Besides the much better capacity retention, the cells with protected Na-anodes feature much lower cell polarization defined as a difference between cell charge and discharge at the half of the entire capacity value. Thus, the cell polarization for the 100th cycle corresponds to about 0.4 V for the cell with non-protected Na and 0.28 V for the cell with NaOH-protected Na. The discrepancy between cells becomes even larger with the cycling, giving 1.8 V for the cell with the bare Na and only 0.55 V for the cell with NaOH-Na after 500 cycles.

The increase in cell polarization correlates with an increase in cell resistance. This internal resistance is an indicator of the formation of passive components at the electrodes, as for example “dead” Na. The electrochemically active surface area is reduced, and less sodium can be stripped off to be intercalated into the cathode material. The passivated sodium surface cannot completely suppress the formation of “dead” Na, but its formation is slowed down.

Note that after disassembling the full-cells, the unprotected sodium could not be isolated from the separator due to a strong adhesion/growing into the separator space. In contrast, the protected sodium could be easily isolated from the separator, keeping its white surface.

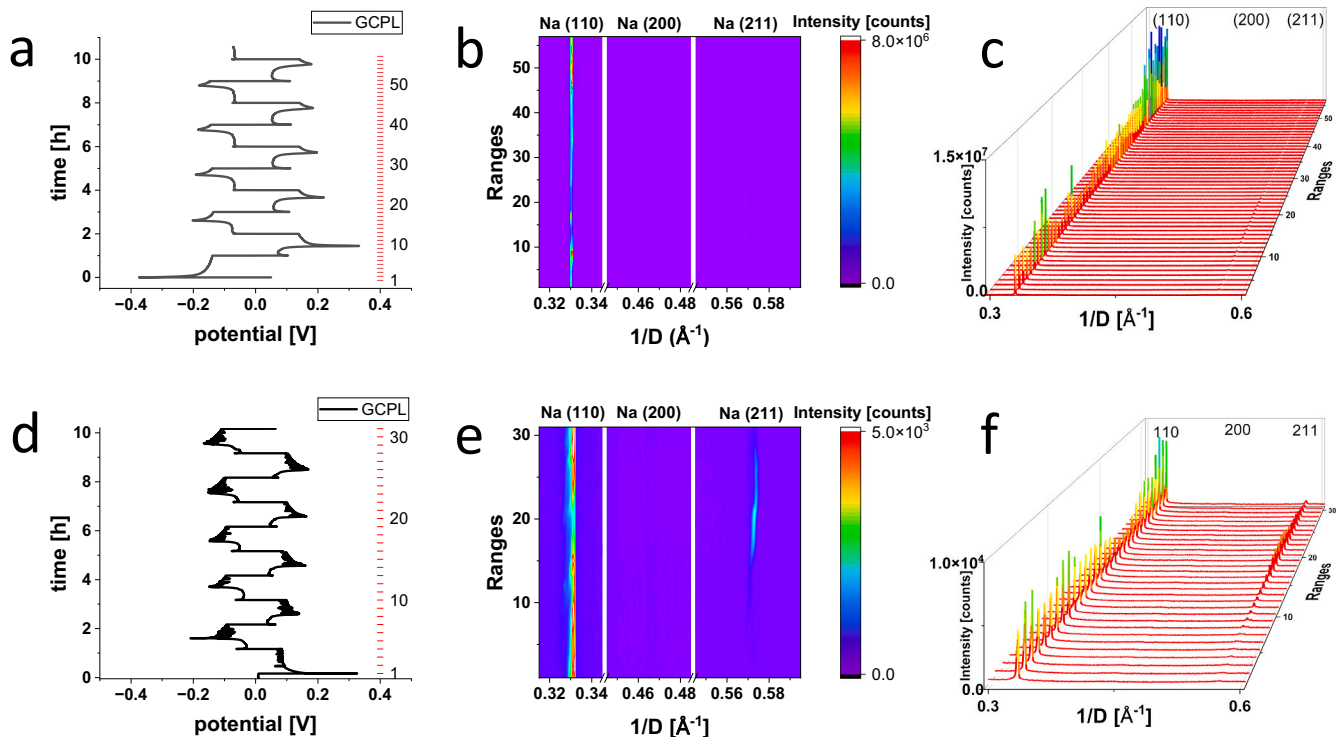

Fig. 7. (a-c) Operando XRD of a Na ‖ Na (NaOH-protected) cell, and (d-f) a symmetric Na ‖ Na (only one side in beam) in comparison, together with the (a, d) GCPL measurement (1 mA/cm^2 current density, 1 mAh/cm^2 capacity), (b,e) counterplot and (c, f) waterfall-plot. From electrochemical point of view, both cells behave similarly. From the structural point of view, there are noticeable differences.

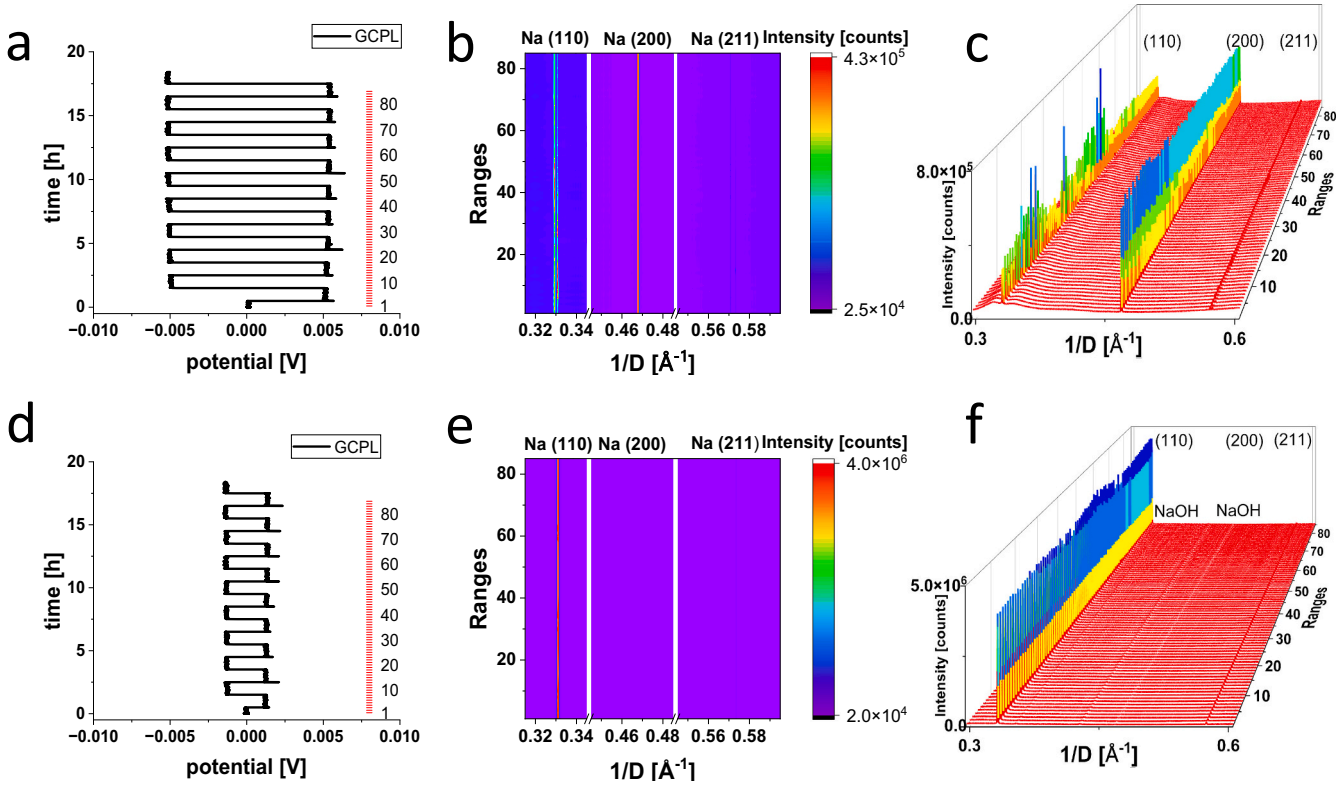

Fig. 8. (a-c) Comparison of bare sodium as electric conductor, with d-f) NaOH passivated sodium as electric conductor, the current density was 1 mA/cm^2, applied for 1 h for positive and negative current. The XRD patterns of NaOH-protected sodium remain nearly unchanged during cycling. The cell voltage is only 1/5 compared to bare sodium.

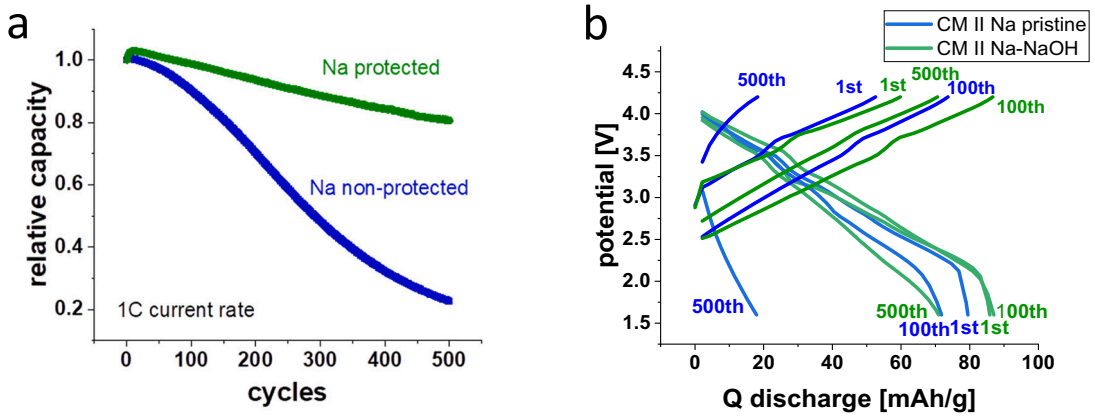

Fig. 9. (a) normalized discharge capacities of full-cells with bare Na (blue) and NaOH-protected Na (green). (b) charge-discharge capacities of the 1st, 10th, 50th, 100th and 500th cycle (1C current density, 256 mA/g).

(see Section 6 in the supplement). Therefore, the NaOH-protected sodium could significantly suppress the volume changes and "dead" Na formation during cycling.

Further, the focus was put on structural changes in the Na-anode during discharge using *operando* XRD in a cell with the $Na_{0.7}Co_{0.8}Ti_{0.2}O_2$ cathode. In both cells, with bare Na and NaOH-passivated Na, the active cathode material was put outside the beam (Fig. 10).

The discharge curve for both cells looks quite similar, as expected for the first cycle. The main difference is in morphology changes of pristine and protected sodium. In the first cycle, the charge capacity is about 25 % lower than the discharge one. Therefore, upon discharge, Na is partially coming from the bulk metallic Na anode, and the observed structural changes correspond to the Na-stripping from bulk.

In both cells, the (110) reflection of Na is very pronounced at the beginning of discharge at 4.2 V vs. Na^+/Na, pointing to highly oriented Na-fibers formed during the cell charge. Moreover, some splitting of

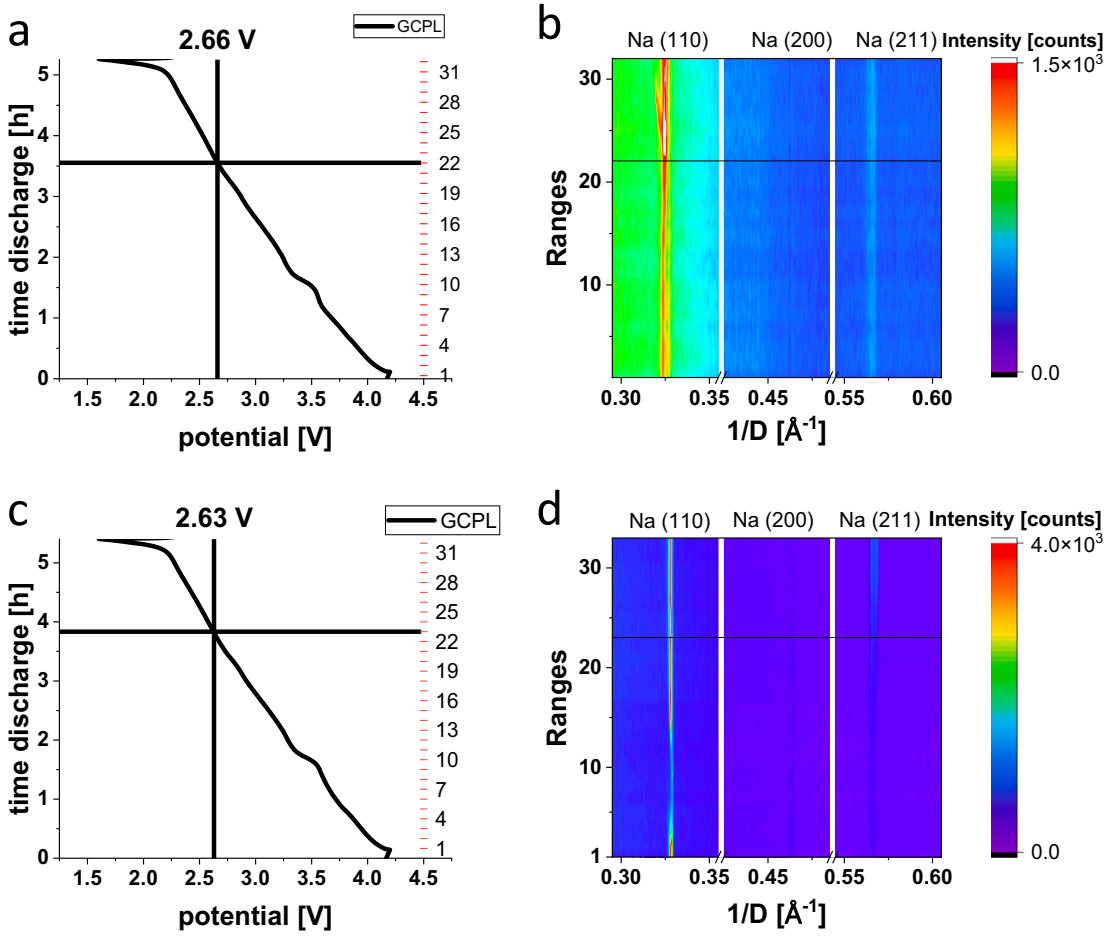

Fig. 10. First discharge curve of a full-cell with non-protected Na (a-b) and protected Na (c-d) as anode, and a $Na_{0.7}Co_{0.8}Ti_{0.2}O_2$ cathode, recorded with C/10 current rate. The GCPL curves are similar, but pristine sodium underwent higher changes in the (110) direction below 2.6 V.

(110) for the non-protected Na probably corresponds to a messy Na-deposition during cell charge. During discharge, the intensity of the (110) peak decreases at the beginning. Below the cell potential of about 2.6 V, Na-stripping from bulk should begin in the assumption of a nearly zero Na-uptake for the SEI formation. For the non-protected Na, the (110) intensity suddenly increases below 2.6 V, and even a second (110) peak appears with a lower 1/D value, revealing a repeated re-crystallization of fibers.

For the protected sodium, the (110) reflection at the beginning of discharge is narrow, confirming a more regular Na-deposition during cell charge. A decrease in the intensity at the beginning of discharge is observed as well. Below about 2.6 V, the (110) intensity significantly increases, however without splitting the reflection. Additionally, the intensity of the (211) reflection is also slightly growing. Probably, some small changes in the Na morphology occur, but they are considerably weaker than in case of the non-protected Na.

Therefore, one can conclude that the NaOH-protection noticeably regulates the Na-stripping behavior, palliating the re-crystallization process of Na-fibers. This uncontrolled re-crystallization of Na-fibers of the non-protected Na is expected to result in "dead"-Na formation within the separator space. In opposite, the NaOH-layer significantly reduces the random growth of Na-fibers in the Na-sub-surface region.

4. Discussion

In contrast to the work describing rather negative properties of a NaOH layer, formed on the Na-surface through the reaction with water vapor [42], with our air-formed NaOH protection on the top of the Na metal anode, we were able to achieve a significant improvement of the cycling stability in half and full Na-cells. The difference between the NaOH layers from the work [42] and our results can be caused by a different layer thickness and Na-morphology. Thus, treatment of metallic Na with a water vapor leads to a denser layer with a thickness of ~5 μm, directly contacting metallic sodium. In contrast, we created a NaOH layer with a thickness lower than 1 μm with a fibrous Na-structure between this layer and the surface of bulk metallic sodium. Apparently, the reaction mechanisms are different. Exposure to water vapor is obeyed to a zero-order chemical reaction [61], which is independent of the reactant concentration and continues until the reactant has been exhausted. Therefore, the thickness of the formed NaOH layer cannot be reliably controlled, in contrast to the reaction of Na with air components, which represents a first-order chemical reaction [41].

A first order reaction, as a concentration dependent reaction, enables a more controllable NaOH growth on the top of metallic Na. Probably both parameters, the thinner NaOH-layer and the fibrous structure in the sub-surface region facilitating Na-diffusion, are necessary to achieve a stable long-term cycling. Further structural investigations like operando NMR, texture analysis, ex situ TEM and ex situ SEM-FIB are necessary to deeper investigate the passivation layer during and after cycling.

The produced NaOH layer fulfills properties, which are required for a stable anode in Na-batteries. It withstands an exposure against the reactive electrolyte, at least for one week, without changes in morphology of the layer or the metallic sodium. Recrystallization, a phenomenon easily happening in metallic sodium, is suppressed and the original morphology of the passivated sodium is intact.

Even without a direct measurement of the ionic conductivity and diffusion barrier for the passivated sodium, it is obvious that the passivated sodium has a lower overpotential as an electric conductor, without any changes in morphology due to the current flow. Changes during cycling in the electrolyte solution are limited to the (110) direction, which means that although some recrystallization of highly oriented fibers takes place, it is much less pronounced than in the case of non-protected metallic sodium. The inner ohmic resistance remains small allowing an assumption that there is no significant volume change on the anodic side upon battery operation.

All this leads to a stable discharging behavior in a full-cell, especially at voltages when Na-stripping from the bulk metallic Na starts to occur. This is a critical point for the long-term cycling stability, since the anode degradation, being a consequence of the random Na-recrystallization, seems to be more pronounced during the cell discharge. A thin, mechanically and chemically stable protective layer on the Na metal anode acts as a guide for a controllable Na-removal.

As mentioned above, the preparation method of the protective layer on sodium is a very critical aspect. This especially includes the exposition time of metallic sodium to ambient conditions in order to avoid the formation of $NaHCO_3$ and Na_2CO_3, which have a higher solubility in carbonate-based electrolyte solutions. Moreover, mechanical pre-treatment of Na may influence its properties as metal anode as well. Thus, only rolled sodium showed a good electrochemical behavior, while pressed sodium, with mostly containing isolated fibers (very intense (200) reflection in the XRD pattern) and/or cubes (very intense (211) direction) shows a worse performance in electrochemical cells (see Section 1 in the supplement).

So far, we did only the first step to connect structural properties of bare and protected Na metal anode and its performance in symmetric, half and full-cells. However, further investigations are necessary to evaluate the aging process on the anode side from the structural point of view.

5. Conclusion

As a conclusion of this work, a thin NaOH layer on top of the metallic sodium can be easily formed by exposure of the metal to ambient conditions. This protected sodium demonstrates a noticeably enhanced electrochemical performance in Na-batteries. As a result, the Na ‖ Na (NaOH-protected) half-cell lasts eight times longer than a symmetric Na ‖ Na cell. The NaOH layer suppresses side reactions between the sodium and electrolyte, as wells as big changes in Na-morphology (recrystallization) caused by current flow. As a result, a full-cell with a $Na_{0.8}Co_{0.8}Ti_{0.2}O_2$ cathode and a NaOH-protected Na-anode revealed a capacity retention of 81 % after 500 cycles at 1C in a Swagelok cell, while the cell with non-protected Na delivered only 20–22 % capacity retention.

Since the formation of the passivation layer takes place under normal atmosphere, the procedure could be easily integrated into a production process. The processed Na on the Al-foil only needs to be exposed for a defined time period to air, and the protection layer appears. The passivated sodium can be directly used as an anode in batteries with 1 M $NaClO_4$-containing electrolyte solution.

CRediT authorship contribution statement

Alexander Thomas: Conceptualization, Methodology, Investigation, Data curation, Visualization, Writing – original draft. **Björn Pohle:** Methodology, Investigation, Validation. **Johannes Schultz:** Investigation, Formal analysis. **Martin Hantusch:** Investigation, Formal analysis. **Daria Mikhailova:** Writing – review & editing, Supervision, Project administration, Funding acquisition.

Declaration of competing interest

The authors declare that they have no known competing financial interests or personal relationships that could have appeared to influence the work reported in this paper.

Data availability

Data will be made available on request.

Acknowledgment

This work was supported by the *Bundesministerium für Bildung und*

Forschung and is carried out as part of the HeNa project (03XP0390C).

Johannes Schultz thanks the HORIZON EUROPE framework program, grant number 101094299, for the financial support.

The authors would like to thank Thomas Wiek (IFW Dresden) for the SEM-FIB measurements, Dr. Alexander Missyul for the support at the MSPD beamline at ALBA synchrotron in Barcelona, Spain, and Andrea Voß and Anne Voidel (both IFW Dresden) for the ICP-OES analysis.

Appendix A. Supplementary data

SI contains operando XRD data for pressed NaOH-protected Na in a half-cell, XPS data for some reference materials, SEM-FIB of protected sodium and SEM of cycled protected sodium. Supplementary data to this article can be found online at doi: https://doi.org/10.1016/j.est.2023.109900.

References

[1] B. Dunn, H. Kamath, J.M. Tarascon, Science 334 (2011) 928.
[2] Z.G. Yang, et al., Chem. Rev. 111 (2011) 3577.
[3] D.A. Stevens, J.R. Dahn, J. Electrochem. Soc. 147 (4) (2000) 127.
[4] M. He, R. Davies, et al., J. Power Sources 548 (2022), 232036.
[5] L.-F. Zhao, et al., Adv. Energy Mater. 11 (2020) 2002704.
[6] J. Wang, et al., J. Phys. Chem. 111 (2007) 14925–14931.
[7] Y. Xu, et al., Chem. Commun. 49 (2013) 8973–8975.
[8] Z. Liang, et al., Chin. Phys. B 21 (2012), 028201.
[9] A. Rudola, et al., Chem. Commun. 49 (2013) 7451–7453.
[10] K. Cao, et al., Small 12 (2016) 2991–2997.
[11] P. Senguttuvan, et al., Chem. Mater. 23 (2011) 4109–4111.
[12] Y. Cao, et al., Adv. Funct. Mater. 30 (2020) 2003733.
[13] C. Wu, et al., Adv. Sci. 5 (2018) 1800519.
[14] L. Li, et al., Energy Environ. Sci. 11 (2018) 2310–2340.
[15] Q. Lu, et al., Appl. Surf. Sci. 60 (2022), 154168.
[16] Y.M. Chang, et al., Mater. Today Adv. 6 (2020), 100054.
[17] G. Eda, et al., Nano Lett. 11 (2011) 5111–5116.
[18] M. Acerce, et al., Nat. Nanotechnol. 10 (2015) 313–318.
[19] X.M. Geng, et al., Adv. Funct. Mater. 27 (2017) 1700998.
[20] W.S. Xiong, et al., Chem. Commun. 54 (2018) 9406–9409.
[21] Q. Shi, et al., Angew. Chem. Int. Ed. Eng. 57 (2018) 9069–9072.
[22] B. Sun, et al., Adv. Mater. 30 (2018) 1801334.
[23] N. Tapia-Ruiz, et al., J. Phys. Energy 3 (2021), 031503.
[24] L. Ma, et al., Energy Storage Mater. 27 (2020) 522–554.
[25] H. Kim, G. Jeong, et al., Adv. Energy Mater. 6 (2016) 1600862.
[26] G. Bieker, M. Winter, P. Bieker, Phys. Chem. Chem. Phys. 17 (2015) 8670–8679.
[27] H. Wang, et al., Chem. Soc. Rev. 49 (2020) 3783–3805.
[28] H. Wang, et al., Chem 5 (2019) 313–338.
[29] Z.X. Xu, et al., Adv. Funct. Mater. 29 (2019) 1901924.
[30] Y. Xie, et al., Nano Res. 16 (2023) 2436–2444.
[31] Y. Zhao, et al., Nano Lett. 17 (2017) 5653–5659.
[32] P. Shi, et al., Batteries 9 (2023) 345.
[33] J. Sun, et al., Electrochim. Acta 20 (2019) 18–24.
[34] Q. Lu, et al., Mater. Lett. 275 (2020), 128206.
[35] T. Li, et al., Adv. Energy Mater. 11 (2020) 2003699.
[36] S.J. An, J. Li, C. Daniel, et al., Carbon 105 (2016) 52–76.
[37] M.J. Wang, et al., Materialia 12 (2020), 100792.
[38] J.D. McBrayer, et al., Nanotechnology 32 (2021), 502005.
[39] H. Stehr, Z. Kristallogr. 125 (1967) 332–359.
[40] I.E. Hooton, P.W.M. Jacobs, Can. J. Chem. 66 (1988) 830.
[41] B.L. Herrington, J. Phys.Chem. 38 (1934) 675–682.
[42] S. Yamaguchi, Nature 145 (1940) 742.
[43] S. Yamaguchi, Bull. Inst. Phys. Chem. Res. 21 (1942) 399/404.
[44] S. Yamaguchi, Bull. Chem. Soc. Japan 18 (1943) (424/34).
[45] S. Yamaguchi, Japan Sci. Rev. 1 (1949) 24–31.
[46] A.L. Smith, et al., J. Chem. Thermodyn. 114 (2017) 93–115.
[47] J.W. Moyer, Phys. Rev. 83 (1951) 877.
[48] J.W. Moyer, Bull. Am. Phys. Soc. 26 (4) (1951) 13.
[49] W.H. Howland, L.F. Epstein, Ind. En. Chem. 49 (11) (1957) 1931–1932.
[50] B. Pohle, et al., Energies 15 (2022) 3371.
[51] L.W. Barr, J.N. Mundy, F.A. Smith, The philosophical magazine: a journal of theoretical experimental and applied, Physics 16 (1967) 1139–1146.
[52] P.W. Stephens, J. Appl. Crystallogr. 32 (1999) 281–289.
[53] C. Goria, Kolloid-Zeitschrift 89 (1939) 325/8.
[54] A.W. Hull, Phys. Rev. 10 (1917) 661–696.
[55] R.W.G. Wyckoff, I. Crystal Structures, Second Edition, Interscience Publishers, New York, 1963.
[56] A. Barrie, F.J. Street, J. Electron Spectrosc. Relat. Phenom. 7 (1975) 1–31.
[57] P.H. Citrin, Phys. Rev. B 8 (1973) 5543.
[58] I.L. Dillamore, W.T. Robers, Acta Metall. 12 (1964) 281–293.
[59] L.A.I. Kestens, H. Pirgazi, Mater. Sci. Technol. 32 (2016) 1303–1315.
[60] B. Baker, Proc. Phys. Soc. Lond. 25 (1912) 235.
[61] N. Stavreska, V. Petruševski, V. Ivanovski, Chem. Educ. 15 (2010) 321–324.